Scuola di Dottorato Leonardo da Vinci – a.a. 2007/08

LASER: CARATTERISTICHE, PRINCIPI FISICI, APPLICAZIONI

Versione 1 – Luglio 08 – http://www.df.unipi.it/~fuso/dida

Parte 5
Cavità, perdite, gudagno ed oscillazione laser

SOMMARIO

Abbiamo ottenuto amplificazione di radiazione da mezzi attivi pompati, ma cosa ne facciamo?

- Da amplificatore ad oscillatore: retroazione e cavità risonante:
  - guadagno e perdita
  - un po' di ottica (soprattutto diffrazione)

- Modi longitudinali e trasversali:
  - richiami
  - operazione multimodo e singolo modo

Obiettivo : individuare l'altro componente essenziale per il laser, la cavità

Obiettivo secondario: porre le basi per spiegare caratteristiche luce laser in condizioni "reali" e per strategie di miglioramento da vedere in seguito

AMPLIFICATORE/OSCILLATORE

Attenzione:
mezzo attivo con inversione (pompaggio) è amplificatore, ma non ancora LASER

Amplificatore → Oscillatore: RETROAZIONE (feedback)

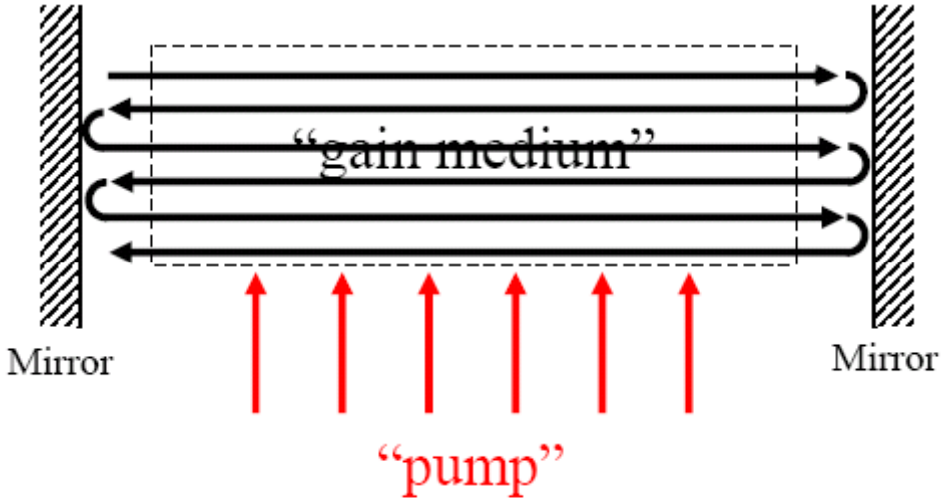

Altro ingrediente fondamentale del laser:
RISONATORE OTTICO (cavità)

Il mezzo attivo (pompato) deve essere contenuto in un'opportuna cavità ottica che permette:
- feedback → emissione
- controllo proprietà spettrali → selezione modi fotonici da amplificare

CAVITÀ LASER

Cavità ideale a 4 specchi (tre perfetti, uno semiriflettente)

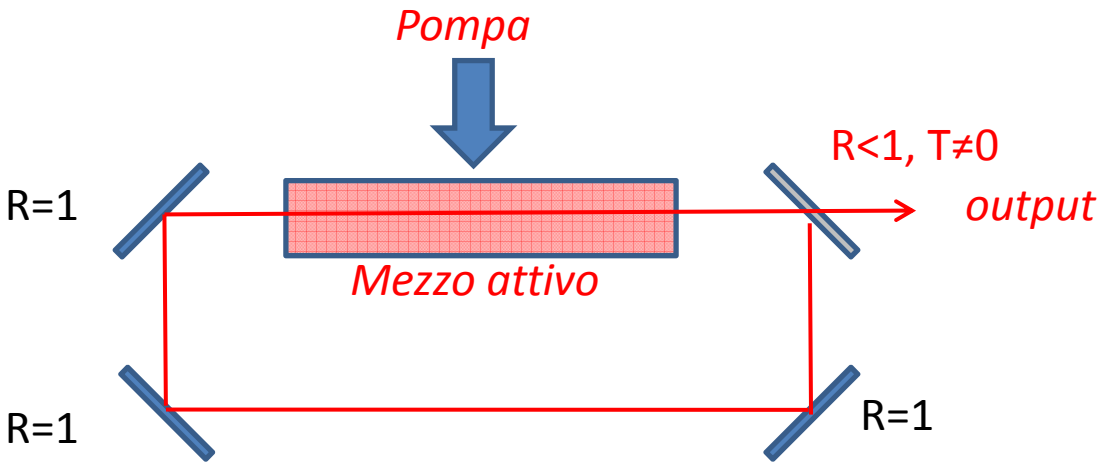

Roundtrip time $\tau \sim L/c$
(L lunghezza totale)

Innesco laser: fotone emesso per emissione spontanea che viaggia nella cavità

$$\frac{dE}{dt} = -E\beta \rightarrow E(t) = E_0 e^{-t\beta}$$

E : energia e.m. nella cavità
β : rate di perdita energia

Fattore di qualità: $Q = 2\pi E_{stored} / E_{lost\ per\ cycle}$

$$Q = 2\pi\beta c/\lambda = \omega/\beta$$

CAVITÀ IDEALE E PERDITE

Energia nella cavità: *SLu*
Intensità (modulo vettore si Poyting) sullo specchio di uscita:
I = Scu , con *S* sezione geometrica della cavità, *c* velocità della luce

Intensità persa dallo specchio di uscita:
I' = Scu(1-R) , con *R* riflettività dello specchio

Energia persa per ciclo:
$E' = I' \lambda/c = Scu(1-R)\lambda/c = S\lambda u(1-R)$

Fattore di qualità della cavità:
$Q = 2\pi SLu/((1-R)S\lambda u) = 2\pi(L/\lambda)/(1-R)$

Esempio:
L = 50 cm, R = 0.98, λ = 0.6 μm → Q ~ $2x10^7$ (HeNe)
L = 0.5 mm, R = 0.30, λ = 0.8 μm → Q ~ $6x10^3$ (diode)

Qualsiasi cavità laser, a causa del fatto che si vuole fare uscire parte della radiazione, possiede perdite

↓

Fattore di qualità finito

Per emissione laser occorre che: *rate di guadagno G > rate di perdita Q*
EQ > EG → Q > G (per alti guadagni basta piccolo *Q* e viceversa)

PERDITE E GUADAGNO SISTEMA A 3 LIVELLI

Guadagno del mezzo attivo (sistema a tre livelli, da master equation):

$$\mathcal{G} = \frac{R\left(2A_{32}+A_{21}\right)-A_{21}\left(A_{31}+A_{32}\right)}{A_{21}\left[A_{31}+A_{32}\right]}\left(\frac{c}{n}\right)\frac{N\,\hbar\,\omega\,B_{21}\,F(\omega)}{V}$$

For $I_0 << I_{sat}$ $I(z,\omega) = I_0 \exp(\mathcal{G} z)$ "Inverse Beer's Law"

For $I_0 >> I_{sat}$ $I(z,\omega) = I_0 + I_{sat}\,\mathcal{G} z$ Linear regime

Now consider elementary laser operation with feedback provided by two mirrors separated by a distance L. We first calculate the famous formula for ***threshold gain*** from the following consistency condition:

$$I_0 \exp(-\alpha 2L)\exp(\mathcal{G}_{th} 2L)\, r_1 r_2 = I_0 \qquad [\text{V-9a}]$$

or

$$\boxed{\mathcal{G}_{th} = \alpha + \frac{1}{2L}\ln\left(\frac{1}{r_1 r_2}\right)} \qquad [\text{V-9b}]$$

Cavità a due specchi r_1, r_2
Separazione L
Ulteriori perdite con rate α

where α is included to account for residual cavity losses and the r_j's are the respective reflectivity's of the two mirrors. At high power -- *i.e.* at powers well above threshold -- the consistency condition becomes (neglecting residual absorption)

PERDITE E GUADAGNO II

$$I_{\nu} \approx r_1 r_2 \left[I_{\nu} + I_{sat} \mathcal{G} 2L \right] \qquad [\text{V-10a}]$$

$$I_{\nu} \approx 2 I_{sat} \mathcal{G} L \left[\frac{1}{r_1 r_2} - 1 \right]^{-1} \qquad [\text{V-10b}]$$

From Equation [V-7b] we may write

$$\frac{\mathcal{G}}{\mathcal{G}_{th}} = \frac{R - R_{\nu}}{R_{th} - R_{\nu}} \qquad [\text{V-11a}]$$

where

Rate di perdita (cavità+em. spont.)

Rate di guadagno del mezzo attivo

$$R_{\nu} = \frac{A_{21}\left(A_{31} + A_{32}\right)}{\left(2A_{32} + A_{21}\right)} \quad \text{and} \quad R_{th} - R_{\nu} = \mathcal{G}_{th} \frac{A_{21}\left[A_{31} + A_{32}\right]}{\left(2A_{32} + A_{21}\right)} \left(\frac{n}{c}\right) \frac{V}{N \hbar \omega B_{21} F(\omega)} \qquad [\text{V-11b}]$$

Therefore Equation [V-10b] becomes

$$I_{\nu}(R) \approx \frac{2 I_{sat} \mathcal{G}_{th} L}{\left[\frac{1}{r_1 r_2} - 1\right]} \left\{ \frac{R - R_{\nu}}{R_{th} - R_{\nu}} \right\} = \left\{ \frac{2 I_{sat} \mathcal{G}_{th} L}{\left[\frac{1}{r_1 r_2} - 1\right]\left[R_{th} - R_{\nu}\right]} \right\} \left(R - R_{\nu}\right) = C\left(R - R_{\nu}\right) \qquad [\text{V-12}]$$

SOGLIA DI EMISSIONE LASER

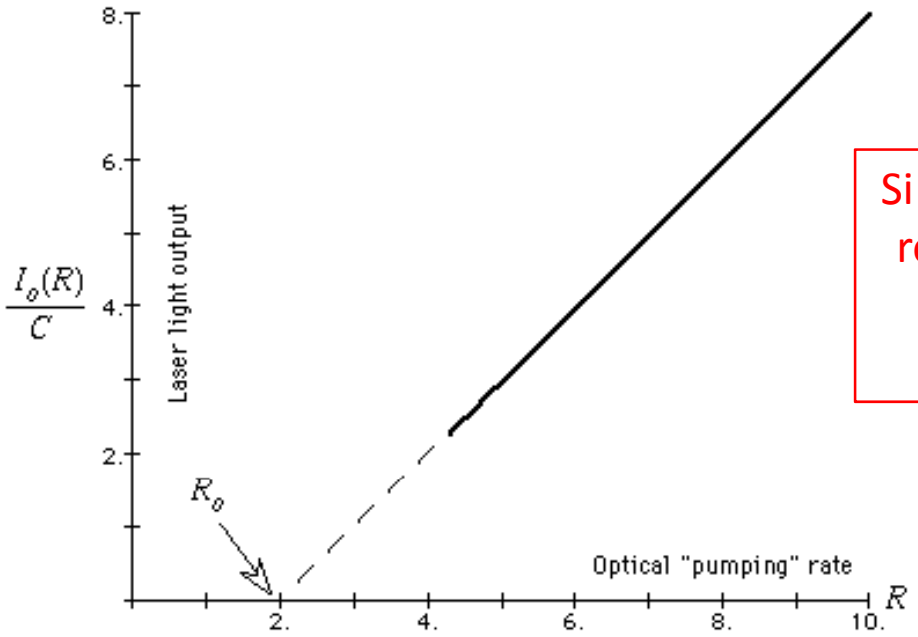

Si ha emissione laser solo se il guadagno (per roundtrip) supera le perdite (per roundtrip)

⇓

Soglia nel rate di pompaggio *R*

Nei laser in cui il rate di pompaggio può essere controllato dall'esterno l'andamento si ritrova quasi esattamente (esempio: laser a diodo, dove il pompaggio dipende dalla corrente di iniezione)

ALTRE PERDITE: DIFFRAZIONE I

10.1.3 Several Coherent Oscillators

As a simple yet logical bridge between the studies of interference and diffraction, consider the arrangement of Fig. 10.6. The illustration depicts a linear array of N coherent point oscillators (or radiating antennas), which are each identical even to their polarization. For the moment, consider the oscillators to have no intrinsic phase difference, i.e. they each have the same epoch angle. The rays shown are all almost parallel, meeting at some very distant point P. If the spatial extent of the array is comparatively small, the separate wave amplitudes arriving at P will be essentially equal, having traveled nearly equal distances, that is

$$E_0(r_1) = E_0(r_2) = \cdots = E_0(r_N) = E_0(r).$$

The sum of the interfering spherical wavelets yields an electric field at P, given by the real part of

$$E = E_0(r)e^{i(kr_1 - \omega t)} + E_0(r)e^{i(kr_2 - \omega t)} + \cdots + E_0(r)e^{i(kr_N - \omega t)}. \tag{10.1}$$

It should be clear, from Section 9.1, that we need not be concerned with the vector nature of the electric field for this configuration. Now then

$$E = E_0(r)e^{-i\omega t}e^{ikr_1}[1 + e^{ik(r_2 - r_1)} + e^{ik(r_3 - r_1)} + \cdots + e^{ik(r_N - r_1)}].$$

The phase difference between adjacent sources is obtained from the expression $\delta = k_0\Lambda$ and since $\Lambda = nd\sin\theta$, in a medium of index n, $\delta = kd\sin\theta$. Making use of Fig. 10.6, it follows that $\delta = k(r_2 - r_1)$, $2\delta = k(r_3 - r_1)$ etc. Thus the field at P may be written as

$$E = E_0(r)e^{-i\omega t}e^{ikr_1}[1 + (e^{i\delta}) + (e^{i\delta})^2 + (e^{i\delta})^3 + \cdots (e^{i\delta})^{N-1}]. \tag{10.2}$$

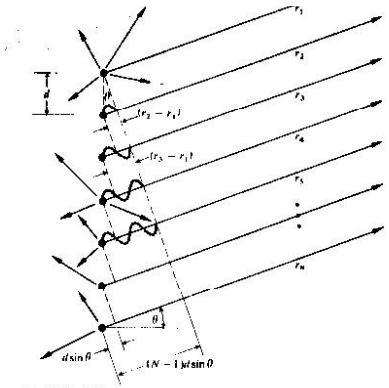

Fig. 10.6 A linear array of in-phase coherent oscillators. Note that at the angle shown $\delta = \pi$ while at $\theta = 0$ δ would be zero.

The bracketed geometric series has the value

$$(e^{iN\delta} - 1)/(e^{i\delta} - 1)$$

which can be rearranged into the form

$$\frac{e^{iN\delta/2}[e^{iN\delta/2} - e^{-iN\delta/2}]}{e^{i\delta/2}[e^{i\delta/2} - e^{-i\delta/2}]}$$

or equivalently

$$e^{i(N-1)\delta/2}\left[\frac{\sin N\delta/2}{\sin\delta/2}\right].$$

The field then becomes

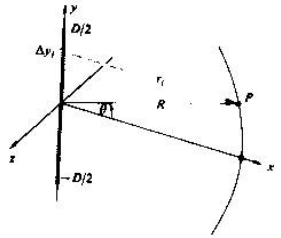

Fig. 10.8 A coherent line source.

$$E = E_0(r)e^{-i\omega t}e^{i[kr_1 + (N-1)\delta/2]}\left(\frac{\sin N\delta/2}{\sin\delta/2}\right). \tag{10.3}$$

Notice that if we define R to be the distance from the center of the line of oscillators to the point P, that is

$$R = \tfrac{1}{2}(N-1)d\sin\theta + r_1,$$

then Eq. (10.3) takes on the form

$$E = E_0(r)e^{i(kR - \omega t)}\left(\frac{\sin N\delta/2}{\sin\delta/2}\right). \tag{10.4}$$

Finally, then, the flux-density distribution within the diffraction pattern due to N coherent, identical, distant point sources in a linear array is proportional to $EE^*/2$ for complex E or

$$I = I_0\frac{\sin^2(N\delta/2)}{\sin^2(\delta/2)}, \tag{10.5}$$

where I_0 is the flux density from any single source arriving at P (see Problem 10.2 for a graphical derivation of the irradiance). For $N = 0$, $I = 0$, for $N = 1$, $I = I_0$, and for $N = 2$, $I = 4I_0\cos^2(\delta/2)$ in accord with Eq. (9.6). The functional dependence of I on θ is more apparent in the form

$$I = I_0\frac{\sin^2[N(kd/2)\sin\theta]}{\sin^2[(kd/2)\sin\theta]}. \tag{10.6}$$

The $\sin^2[N(kd/2)\sin\theta]$ term undergoes rapid fluctuations, while the function modulating it, $\{\sin[(kd/2)\sin\theta]\}^{-2}$, varies relatively slowly. The combined expression gives rise to a series of sharp principal peaks separated by small subsidiary maxima. The principal maxima occur in directions θ_m such that $\delta = 2m\pi$ where $m = 0, \pm1, \pm2, \ldots$. Because $\delta = kd\sin\theta$

$$d\sin\theta_m = m\lambda. \tag{10.7}$$

Since $[\sin^2 N\delta/2]/[\sin^2\delta/2] = N^2$ for $\delta = 2m\pi$ (from

DIFFRAZIONE II (FRAUNHOFER)

L'Hôspital's rule) the principal maxima have values $N^2 I_0$. This is to be expected inasmuch as all of the oscillators are in phase at that orientation. The system will radiate a maximum in a direction perpendicular to the array ($m = 0$, $\theta_0 = 0$ and π). As θ increases, δ increases and I falls off to zero at $N\delta/2 = \pi$, its first minimum. Note that if $d < \lambda$ in Eq. (10.7), only the $m = 0$ or zero-order principal maximum exists. *If we were looking at an idealized line source of electron-oscillators separated by atomic distances, we could expect only that one principal maximum in the light field.*

The antenna array of Fig. 10.7 can then transmit radiation in the narrow beam or lobe corresponding to a principal maximum (the parabolic dishes shown reflect into the forward direction and the radiation pattern is no longer symmetrical around the common axis.) Suppose that we have a system in which we can introduce an intrinsic phase shift of ε between adjacent oscillators. In that case

$$\delta = kd \sin\theta + \varepsilon;$$

the various principal maxima will occur at new angles

$$d \sin\theta_m = m\lambda - \varepsilon/k.$$

Concentrating on the central maximum $m = 0$, its orientation θ_0 can be varied at will by merely adjusting the value of ε.

The principle of reversibility, which states that without absorption, wave motion is reversible, leads to the same field pattern for an antenna used as either a transmitter or receiver. The array, functioning as a radio telescope, can therefore be "pointed" by combining the output from the individual antennas with an appropriate phase shift, ε, introduced between each of them. For a given ε the output of the system corresponds to the signal impinging on the array from a specific direction in space.

Figure 10.7 is a photograph of the first multiple radio interferometer designed by W. N. Christiansen and built in Australia in 1951. It consists of 32 parabolic antennas, each 2 m in diameter, designed to function in phase at the wavelength of the 21 cm hydrogen emission line. The antennas are arranged along an east–west baseline with 7 m separating each one. This particular array utilizes the earth's rotation as the scanning mechanism.

Examine Fig. 10.8 which depicts an idealized line source of electron-oscillators (e.g., the secondary sources of the Huygens–Fresnel principle for a long slit whose width is much less than λ illuminated by plane waves). Each point emits a spherical wavelet which we write as

$$E = \left(\frac{\mathcal{E}_0}{r}\right) \sin(\omega t - kr)$$

explicitly indicating the inverse r-dependence of the amplitude. The quantity $\mathcal{E}_0$ is said to be the *source strength*. The present situation is distinct from that of Fig. 10.6 in that now the sources are very weak, their number, N, is tremendously large and the separation between them vanishingly small. A minute, but finite segment of the array Δy_i, will contain $\Delta y_i(N/D)$ sources where D is the entire length of the array. Imagine then that the array is divided up into M such segments, i.e., j goes from 1 to M. The contribution to the electric field intensity at P from the ith segment is accordingly

$$E_i = \left(\frac{\mathcal{E}_0}{r_i}\right) \sin(\omega t - kr_i) \left(\frac{N\Delta y_i}{D}\right)$$

provided that Δy_i is so small that the oscillators within it have a negligible relative phase difference (r_i = constant) and their fields simply add constructively. We can cause the array to become a continuous (coherent) line source by letting N approach infinity. This description, besides being fairly realistic on a macroscopic scale, also allows the use of the calculus for more complicated geometries. Certainly as N approaches infinity, the source strengths of the individual oscillators must diminish to near zero if the total output is to be finite. We can therefore define a constant $\mathcal{E}_L$ as the *source strength per unit length* of the array, that is

$$\mathcal{E}_L \equiv \frac{1}{D} \lim_{N \to \infty} (\mathcal{E}_0 N). \tag{10.8}$$

The net field at P from all M segments is

$$E = \sum_{i=1}^{M} \frac{\mathcal{E}_L}{r_i} \sin(\omega t - kr_i)\, \Delta y_i.$$

For a continuous line source Δy_i can become infinitesimal ($M \to \infty$) and the summation is then transformed into a definite integral

$$E = \mathcal{E}_L \int_{-D/2}^{+D/2} \frac{\sin(\omega t - kr)}{r}\, dy, \tag{10.9}$$

where $r = r(y)$. The approximations used to evaluate Eq. (10.9) must depend on the position of P with respect to the array and will therefore make the distinction between Fraunhofer and Fresnel diffraction. The coherent *optical* line source does not now exist as a physical entity but we will make good use of it as a mathematical device.

10.2 FRAUNHOFER DIFFRACTION

10.2.1 The Single Slit

Return to Fig. 10.8 where now the point of observation is very distant from the coherent line source and $R \gg D$. Under these circumstances $r(y)$ never deviates appreciably from its midpoint value R so that the quantity $(\mathcal{E}_L/R)$ at P is essentially constant for all elements dy. It follows from Eq. (10.9) that the field at P due to the differential segment of the source dy is

$$dE = \frac{\mathcal{E}_L}{R} \sin(\omega t - kr)\, dy, \tag{10.10}$$

where $(\mathcal{E}_L/R)\, dy$ is the amplitude of the wave. Notice that the phase is very much more sensitive to variations in $r(y)$ than is the amplitude so that we will have to be more careful about introducing approximations into it. We can expand $r(y)$, in precisely the same manner as was done in Problem (9.4), to get it as an explicit function of y, thus

$$r = R - y \sin\theta + (y^2/2R) \cos^2\theta + \cdots, \tag{10.11}$$

where θ is measured from the xz-plane. The third term can be ignored so long as its contribution to the phase is insignificant even when $y = \pm D/2$, i.e. $(\pi D^2/4\lambda R) \cos^2\theta$ must be negligible. This will be true for all values of θ when R is adequately large and we again have the Fraunhofer condition. The distance r is then linear in y. Substituting into Eq. (10.10) and integrating leads to

$$E = \frac{\mathcal{E}_L}{R} \int_{-D/2}^{+D/2} \sin[\omega t - k(R - y \sin\theta)]\, dy, \tag{10.12}$$

and finally

$$E = \frac{\mathcal{E}_L D}{R} \frac{\sin[(kD/2) \sin\theta]}{(kD/2) \sin\theta} \sin(\omega t - kR). \tag{10.13}$$

To simplify the appearance of things let

$$\beta \equiv (kD/2) \sin\theta \tag{10.14}$$

so that

$$E = \frac{\mathcal{E}_L D}{R} \left(\frac{\sin\beta}{\beta}\right) \sin(\omega t - kR). \tag{10.15}$$

The quantity most readily measured is the irradiance (forgetting the constants) $I(\theta) = \langle E^2 \rangle$ or

$$I(\theta) = \frac{1}{2} \left(\frac{\mathcal{E}_L D}{R}\right)^2 \left(\frac{\sin\beta}{\beta}\right)^2, \tag{10.16}$$

where $\langle \sin^2(\omega t - kR) \rangle = \frac{1}{2}$. When $\theta = 0$, $\sin\beta/\beta = 1$ and $I(\theta) = I(0)$ which corresponds to the *principal maximum*. *The irradiance resulting from an idealized coherent line source in the Fraunhofer approximation* is then

$$I(\theta) = I(0) \left(\frac{\sin\beta}{\beta}\right)^2, \tag{10.17}$$

or using the *sinc function* (Section 7.9, and Table 1 of the Appendix)

$$I(\theta) = I(0) \operatorname{sinc}^2 \beta.$$

There is symmetry about the y-axis and this expression holds for θ measured in any plane containing that axis.

DIFFRAZIONE III

$a \sim \lambda$

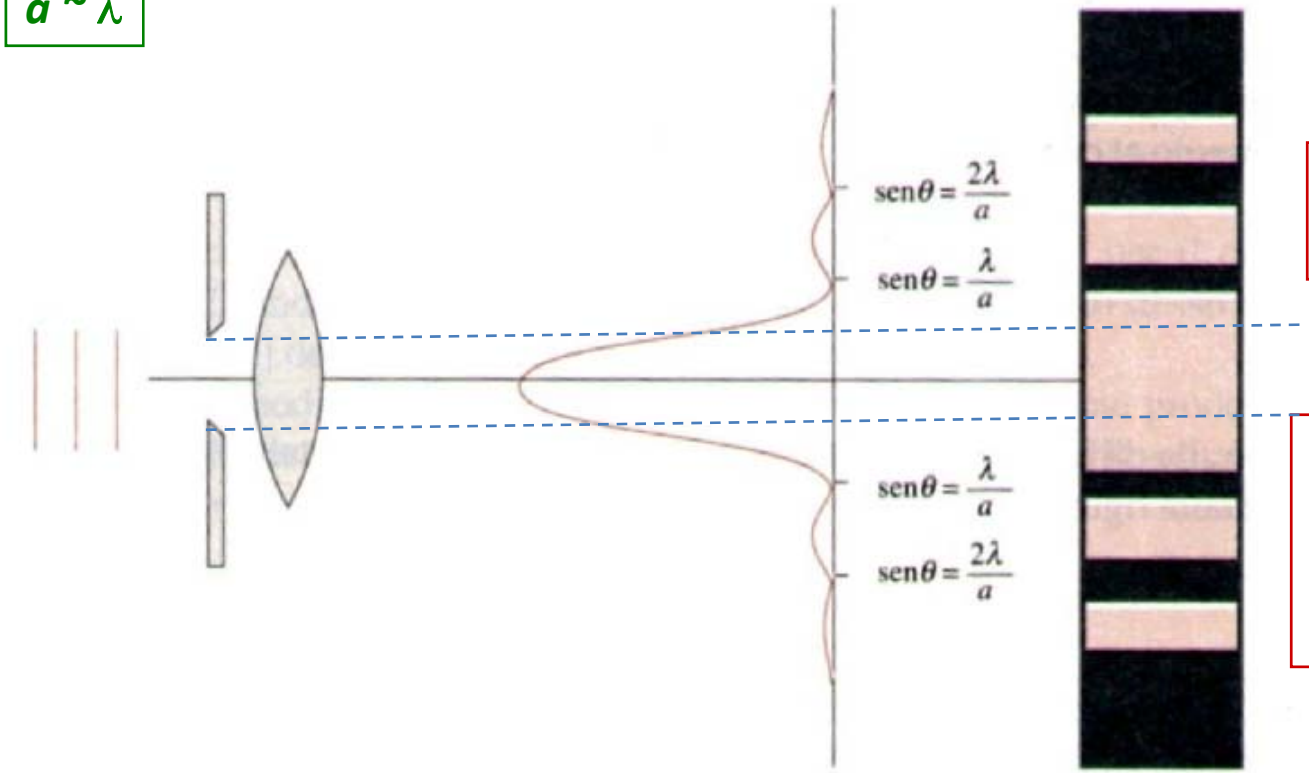

"Diffusion cone":
$\mathrm{Sin}\theta \sim \lambda/a$

Diffraction ripples:
$I \sim I_0 (\sin\alpha/\alpha)^2$
with:
$\alpha = \pi\, a\, \sin\theta \,/\, \lambda$

Il passaggio di luce attraverso un'apertura di diametro $a \sim \lambda$ provoca diffrazione:
- Cono di diffusione;
- Ripples e modulazioni dell'intensità (frange)

DIFFRAZIONE E CAVITÀ

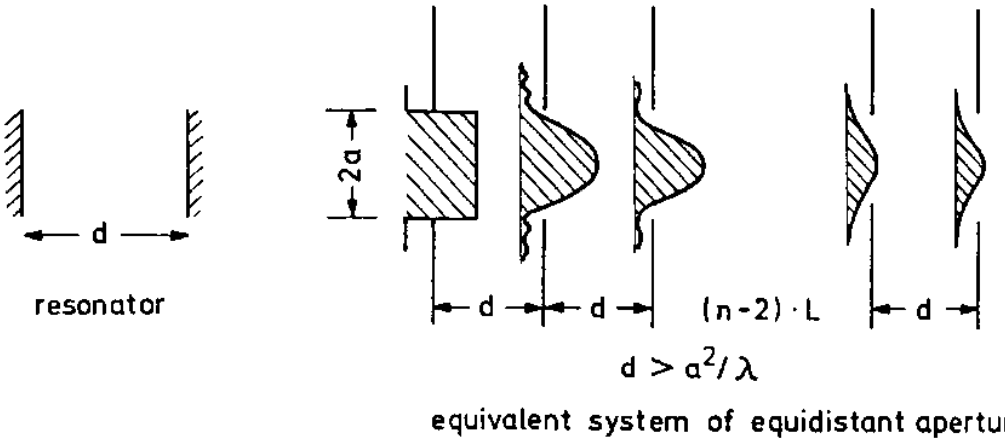

Fig.5.7. The diffraction of an incident plane wave at successive apertures s
d is equivalent to the diffraction by successive reflections in a plane-mirr
with mirror separation d

Per il principio di reciprocità la riflessione da ogni specchio comporta una diffrazione

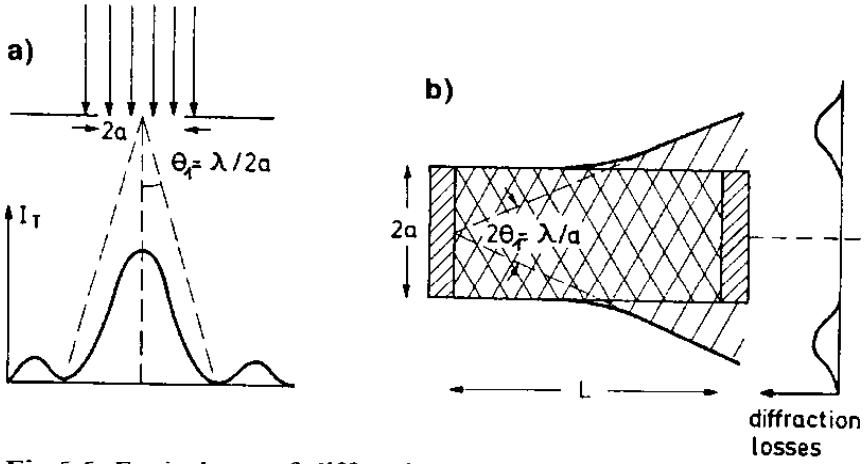

Fig.5.5. Equivalence of diffraction at an aperture (a) and at a mirror of equal size (b). The diffraction pattern of the transmitted light in (a) equals that of the reflected light in (b). The case $\theta_1 d = a \rightarrow N = 0.5$ is shown

In ogni tipo di cavità si verificano perdite legate alla diffrazione (risonatore aperto)

MODI TRASVERSALI DEL CAMPO

5.2.2 Spatial Field Distributions in Open Resonators

In Sect.2.1 we have seen that any stationary field configuration in a closed cavity (called a *mode*) can be composed of plane waves. Because of diffraction, plane waves cannot give stationary fields in open resonators, since the diffraction losses depend on the coordinates (x, y) and increase from the axis of the resonator towards its edges. This implies that the distribution A(x, y), which is independent of x and y for a plane wave, will be altered with each round trip for a wave travelling back and forth between the mirrors of an open resonator until it approaches a stationary distribution. Such a stationary field configuration, called a *mode of the open resonator*, is reached when A(x, y) no longer changes its form, although, of course, the losses result in a decrease of the total amplitude, if they are not compensated by the gain of the active medium.

The mode configurations of open resonators can be obtained by an iterative procedure using the Kirchhoff-Fresnel diffraction theory [5.16]. The resonator with two plane, square mirrors is replaced by the equivalent arrangement of apertures with size $(2a)^2$ and a distance d between successive apertures (Fig.5.7). When an incident plane wave is travelling into the z direction its amplitude distribution is successively altered by diffraction, from a constant amplitude to the final stationary distribution $A_n(x, y)$. The spatial distribution $A_n(x, y)$ in the plane of the n^{th} aperture is determined by the distribution $A_{n-1}(x, y)$ across the previous aperture.

From Kirchhoff's diffraction theory we obtain (Fig.5.8)

$$A_n(x,y) = -\frac{i}{2\lambda}\iint A_{n-1}(x',y')\,\frac{1}{\rho}e^{-ik\rho}(1+\cos\theta)\,dx'dy' \,. \qquad (5.26)$$

A stationary field distribution is reached if

$$A_n(x,y) = CA_{n-1}(x,y) \quad \text{with} \quad C = \sqrt{1-\gamma_D}\,e^{i\phi} \,, \qquad (5.27)$$

The amplitude attenuation factor C does not depend on x and y. The quantity γ_D represents the diffraction losses and ϕ the corresponding phase shift, caused by diffraction.

Inserting (5.27) into (5.26) gives the following integral equation for the stationary field configuration

$$A(x,y) = -\frac{i}{2\lambda}(1-\gamma_D)^{-1/2}e^{-i\phi}\iint A(x',y')\,\frac{1}{\rho}e^{-ik\rho}(1+\cos\theta)\,dx'dy' \,. \qquad (5.28)$$

Because the arrangement of successive apertures is equivalent to the plane-mirror resonator, the solutions of this integral equation also represent the stationary modes of the open resonator. The diffraction-dependent phase shifts ϕ for the modes are determined by the condition of resonance, which requires that the mirror separation d equals an integer multiple of $\lambda/2$.

The general integral equation (5.28) cannot be solved analytically and one has to look for approximate methods. For two identical plane mirrors of quadratic shape $(2a)^2$, (5.28) can numerically be solved by splitting it into two one-dimensional equations, one for each coordinate x and y, if the Fresnel number $N = a^2/(d\lambda)$ is small compared with $(d/a)^2$, which means if $a << (d^3\lambda)^{1/4}$. Such numerical iterations for the "infinite strip" resonator have been performed by *Fox* and *Li* [5.18]. They showed that stationary field configurations do exist, and computed the field distributions of these modes, their phase shifts and their diffraction losses.

Risonatore confocale

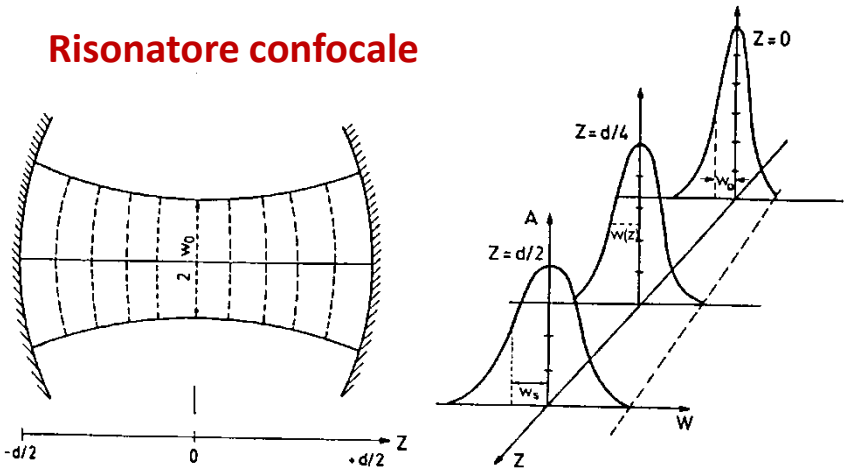

Fig.5.10. Phase fronts and intensity profiles of the fundamental TEM_{00} mode at several locations z in a confocal resonator

La distribuzione spaziale dell'intensità e.m. nella cavità può essere calcolata (numericamente)

RISONATORI CONFOCALI I

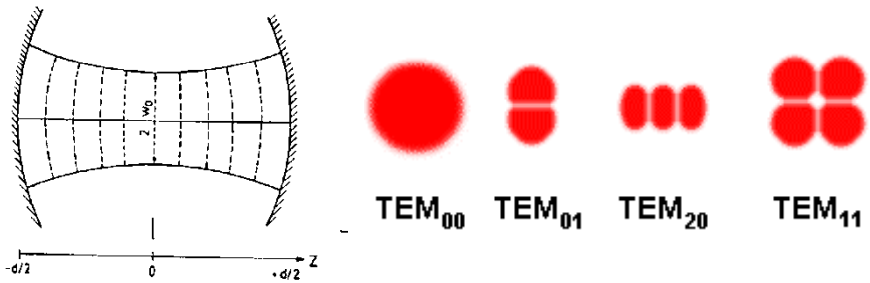

5.2.3 Confocal Resonators

The analysis has been extended by *Boyd, Gordon*, and *Kogelnik* to resonators with confocally-spaced, spherical mirrors [5.19,20] and later by others to general laser resonators [5.21-29]. For the confocal case (mirror separation d is equal to the radius of curvature R), the integral equation (5.28) can be solved with the acceptable approximation a << d, which implies $\rho \approx d$ in the denominator and $\cos\theta \approx 1$. In the phase term $\exp(-ik\rho)$, the distance ρ cannot be replaced by d, since the phase is sensitive already to small changes in the exponent. One can, however, expand ρ into a power series of xx'/d^2 and yy'/d^2. For the confocal case (d = R) one obtains [5.7, 19]

$$\rho \approx d[1 - (xx'+yy')/R^2] \,. \tag{5.29}$$

Inserting (5.29) into (5.28) allows the two-dimensional equation to be separated into two one-dimensional homogeneous Fredholm equations which can be solved analytically [5.19, 23].

From the solutions, the stationary amplitude distribution in the plane z = z_0 vertical to the resonator axis is obtained. For the confocal resonator it can be represented by the product of Hermitian polynomials, a Gaussian function, and a phase factor:

$$A_{mn}(x,y,z) = C^* H_m(x^*) H_n(y^*) \exp(-r^2/w^2) \exp[-i\phi(z,r,R)] \,. \tag{5.30}$$

Here, C^* is a normalization factor. The function H_m is the Hermitian polynomial of m^{th} order. The last factor gives the phase $\phi(z_0,r)$ in the plane z = z_0 at a distance $r = (x^2+y^2)^{1/2}$ from the resonator axis. The arguments x^* and y^* depend on the mirror separation d and are related to the coordinates x, y, z by $x^* = \sqrt{2}x/w$ and $y^* = \sqrt{2}y/w$, where

$$w^2(z) = \frac{\lambda d}{2\pi}[1 + (2z/d)^2] \tag{5.31}$$

is a measure for the radial amplitude distribution.

From the definition of the Hermitian polynomials [5.30], one can see that the indices m and n give the number of nodes for the amplitude A(x,y) in the x (or the y) direction. Figures 5.9,10 illustrate some of these "Transverse Electro-Magnetic standing waves" which are called $TEM_{m,n}$ modes. The diffraction effects do not essentially influence the transverse character of the waves. While Fig.5.9a shows the one-dimensional amplitude distribution A(x) for some modes, Fig.5.9b depicts the two-dimensional field amplitude A(x,y) in Cartesian coordinates and $A(r,\theta)$ in polar coordinates. Modes with m = n = 0 are called *fundamental modes* or *axial modes* (often zero-order transverse modes as well), while configurations with m > 0 or n > 0 are transverse modes of higher order. The intensity distribution of the fundamental mode $I_{00} \propto A_{00}A_{00}^*$ can be derived from (5.30). With $H_0(x^*) = H_0(y^*) = 1$ we obtain

$$I_{00}(x,y,z) = I_0 e^{-2r^2/w^2} \,. \tag{5.32}$$

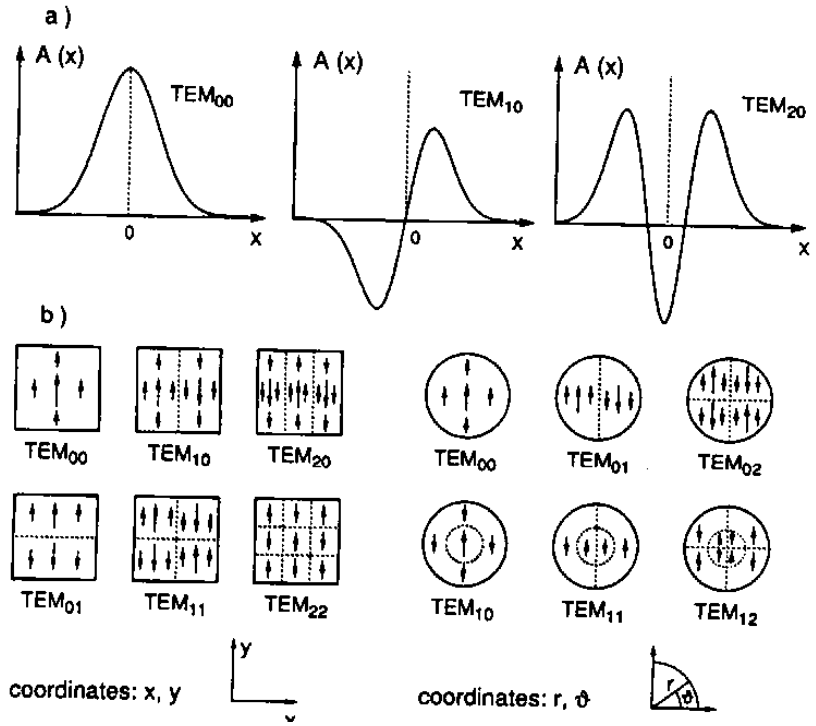

Fig.5.9. (a) Stationary one-dimensional amplitude distributions $A_m(x)$ in a confocal resonator. (b) Two-dimensional presentation of linearly polarized resonator modes for square and circular apertures

RISONATORI CONFOCALI II

The fundamental modes have a Gaussian profile. For r = w the intensity decreases to $1/e^2$ of its maximum value $I_0 = C^{*2}$ on the axis (r = 0). The value r = w is called the *beam radius* or *mode radius*. The smallest beam radius w_0 within the confocal resonator is the *beam waist*, which is located at the center z = 0. From (5.31) we obtain with d = R

$$w_0 = (\lambda R/2\pi)^{1/2} . \qquad (5.33)$$

Waist

At the mirrors (z = d/2) the beam radius $w(d/2) = \sqrt{2}w_0$ is increased by a factor $\sqrt{2}$.

Examples 5.4

a) For a HeNe laser with λ = 633 nm, R = d = 30 cm (5.33) gives w_0 = 0.17 mm for the beam waist.

b) For a CO_2 laser with λ = 10 μm, R = d = 2 m is w_0 = 1.8 mm.

Tipicamente il volume di mezzo attivo "efficace" è molto piccolo

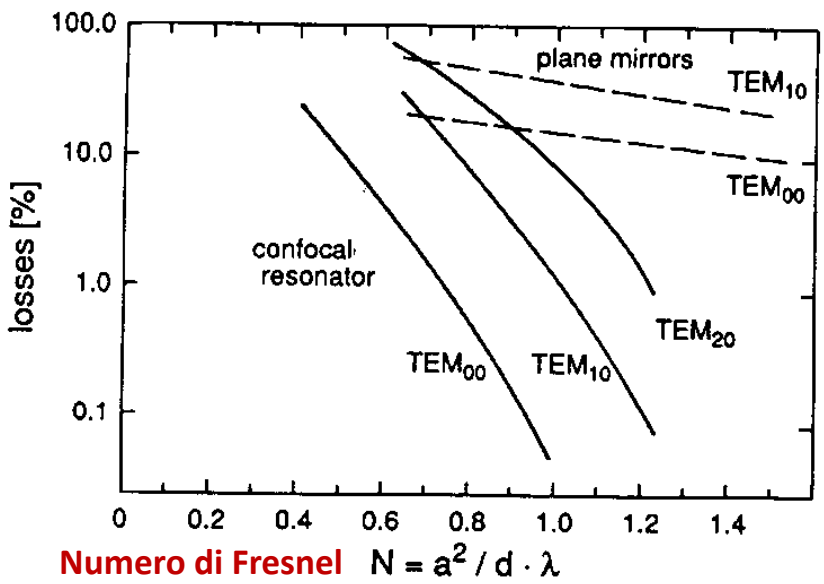

Fig.5.11. Diffraction losses of some modes in a confocal and in a plane-mirror resonator, plotted as a function of the Fresnel number N

A large Fresnel number (well above 1) of a resonator (cavity) means that diffraction losses at the end mirrors are small for typical mode sizes (i.e. not near a stability limit of the resonator, where mode sizes can diverge). This is the usual situation in a stable laser resonator. Conversely, a small Fresnel number means that diffraction losses can be significant – particularly for higher-order modes, so that diffraction-limited operation may be favored.

Il numero di Fresnel è direttamente legato al fattore di qualità, $Q \sim N$

Risonatori confocali permettono di ridurre le perdite, cioè aumentare *Q*, a parità di *N*

STABILITÀ RISONATORI

5.2.6 Stable and Unstable Resonators

In a stable resonator the field amplitude A(x, y) reproduces itself after each round trip apart from a constant factor C which represents the total diffraction losses but does not depend on x or y, see (5.27).

The question is now how the field distribution A(x, y) and the diffraction losses change with varying mirror radii R_1, R_2 and mirror separation d for a general resonator. We will investigate this problem for the fundamental TEM_{00} mode, described by the Gaussian-beam intensity profile. For a stationary field distribution, where the Gaussian beam profile reproduces itself after each round trip one obtains, for a resonator consisting of two spherical mirrors with the radii R_1, R_2, separated by the distance d, the spot sizes πw_1^2 and πw_2^2 on the mirror surfaces [5.1, 23]

$$\pi w_1^2 = \lambda d \left(\frac{g_2}{g_1(1 - g_1 g_2)} \right)^{1/2} ; \quad \pi w_2^2 = \lambda d \left(\frac{g_1}{g_2(1 - g_1 g_2)} \right)^{1/2} \qquad (5.42)$$

with the parameters (i = 1,2)

$$g_i = 1 - d/R_i \, . \qquad (5.43)$$

This reveals that for $g_1 = 0$ or $g_2 = 0$ and for $g_1 g_2 = 1$ the spot sizes become infinite at one or at both mirror surfaces, which implies that the Gaussian beam diverges: The resonator becomes unstable. An exception is the confocal resonator with $g_1 = g_2 = 0$, which is stable if both parameters g_i are exactly zero. For $g_1 g_2 > 1$ or $g_1 g_2 < 0$ the right-hand sides of (5.42) become imaginary, which means that the resonator is unstable. The condition for a stable resonator is therefore

$$\boxed{0 < g_1 g_2 < 1 \quad \text{or} \quad g_1 = g_2 = 0 \, .} \qquad (5.44)$$

Risonatori stabili consentono di ottenere perdite costanti per ogni roundtrip

Risonatori instabili possono essere preferibili per coinvolgere una maggiore quantità di mezzo attivo (fattore di riempimento)
→ Laser ad alta potenza (e scarsa qualità del fascio)

Table 5.1. Some commonly used optical resonators with their stability parameters $g_i = 1 - d/R_i$

Type of resonator	Mirror radii	Stability parameter
Confocal	$R_1 + R_2 = 2d$	$g_1 + g_2 = 2g_1g_2$
Concentric	$R_1 + R_2 = d$	$g_1 g_2 = 1$
Symmetric	$R_1 = R_2$	$g_1 = g_2 = g$
Symmetric confocal	$R_1 = R_2 = d$	$g_1 = g_2 = 0$
Symmetric concentric	$R_1 = R_2 = \frac{1}{2}d$	$g_1 = g_2 = -1$
Semiconfocal	$R_1 = \infty$	$g_1 = 1, g_2 = \frac{1}{2}$
Plane	$R_1 = R_2 = \infty$	$g_1 = g_2 = +1$

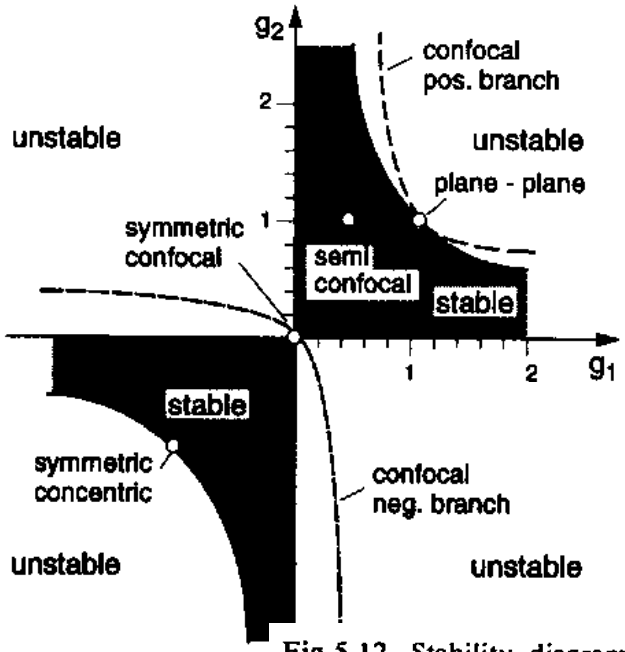

Fig.5.12. Stability diagram of optical resonators. The hatched areas represent stable resonators

RISONATORI E PROPRIETÀ OTTICHE FASCIO

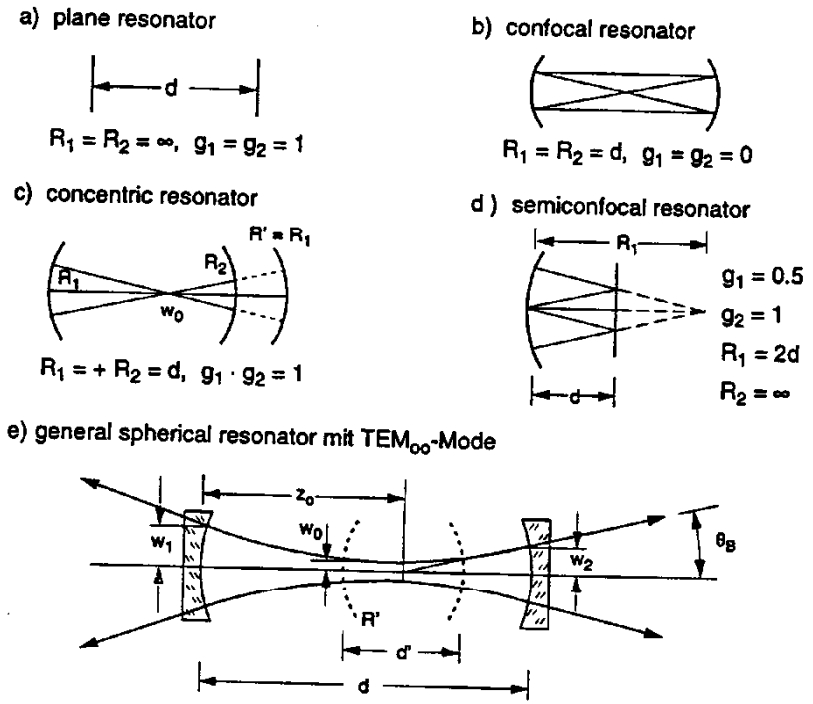

Fig.5.13. Some examples of commonly used

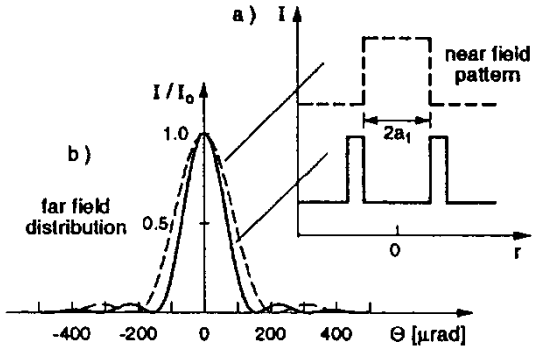

Fig.5.16a,b. Diffraction pattern of the output intensity of a laser with an unstable resonator. (a) Near field just at the output coupler and (b) far-field distribution for a resonator with a = 0.66 cm, $g_1 = 1.21$, $g_2 = 0.85$. The pattern obtained with a circular output mirror (*solid curve*) is compared with that of a circular aperture (*dashed curve*)

For some laser media, in particular those with large gain, unstable resonators with $g_1 g_2 < 0$ may be more advantageous than stable ones for the following reason: In stable resonators the beam waist $w_0(z)$ of the fundamental mode is given by the mirror radii R_1, R_2 and the mirror separation d, see (5.33), and is generally small (Example 5.4). If the cross section of the active volume is larger than πw^2, only a fraction of all inverted atoms can contribute to the laser emission into the TEM_{00} mode, while in unstable resonators the beam fills the whole active medium. This allows extraction of the maximum output power. One has, however, to pay for this advantage by a large beam divergence.

Let us consider the simple example of a symmetric unstable resonator depicted in Fig.5.14 and formed by two mirrors with radii R_i separated by the distance d. Assume that a spherical wave with its center at F_1 is emerging from mirror M_1. The spherical wave geometrically reflected by M_2 has its center in F_2. If this wave, after ideal reflection at M_1, is again a spherical wave with its center at F_1, the field configuration is stationary and the mirrors image the local point F_1 into F_2, and vice versa.

For the magnification of the beam diameter on the way from mirror M_1 to M_2 we obtain from Fig.5.14 the relation

$$M_{12} = \frac{d + R_1}{R_1}. \qquad (5.45)$$

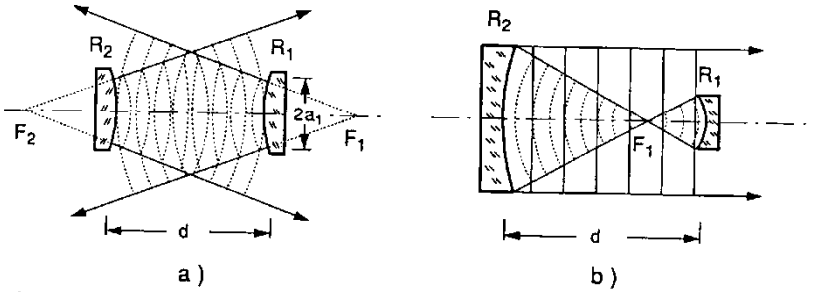

Fig.5.14. (a) Spherical waves in a symmetric unstable resonator, emerging from the virtual focal points F_1 and F_2. (b) Asymmetric unstable resonator with a real focal point between the two mirrors

Proprietà ottiche del fascio
(divergenza, dimensione, fronte d'onda, etc.)
influenzate da geometria cavità

QUALITÀ E ROUNDTRIPS

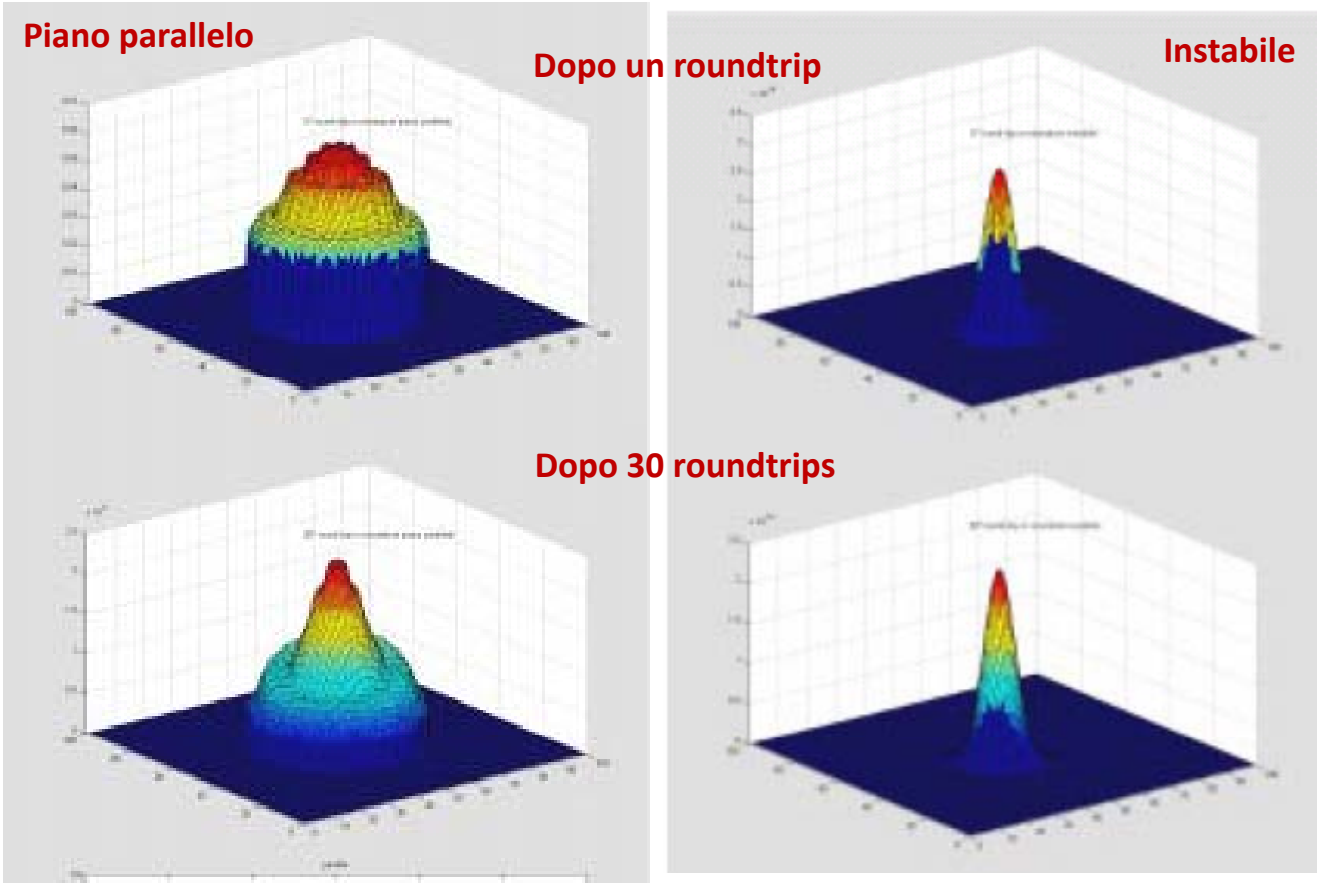

Roundtrip time $\tau \sim L/c$
(L lunghezza totale)

τ [ns] = 3 L [m]

Evoluzione della distribuzione trasversale del fascio al waist

Parametri del fascio	Cavità piano parallela	Cavità instabile
Perdite (%)	45	75
Fattore di qualità	200	10

Tab. 1 – Valori dopo 30 round-trip

Occorrono numerosi passaggi affinché il fascio assuma proprietà ottiche “ottimali”

MODI LONGITUDINALI RISONATORE

Modi lungitudinali

Longitudinal modes involve light waves which travel parallel to the laser cavity axis. When such a wave is reflected from a cavity mirror, the reflected wave combines with the incident wave to give rise to a standing or stationary wave as indicated in Figure 5.1. To simplify the diagram, the amplifying medium has been omitted and, provided that it can sustain several modes of oscillation at the same time, it is not necessary to consider it to understand the origin of multiple longitudinal modes. Amplifying media that can support the simultaneous oscillation of a number of longitudinal modes are referred to as being inhomogeneously broadened.

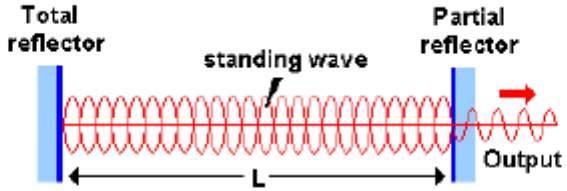

Figure 5.1.

Standing waves can be sustained within the laser cavity only if the length of the cavity is equal to an integral number of half wavelengths. This condition can be written as:

$$nL = s\,\lambda/2, \quad \text{con } s \text{ intero} \qquad (5.1)$$

Quantizzazione modi

Nella 5.1 n indica l'indice di rifrazione del mezzo che riempie la cavità. For most lasers, values of s larger than a million are typical. Because of this, different longitudinal modes corresponding to successive values of s have wavelengths that are different, but only slightly different. It is a simple matter to write down the above condition in terms of the frequency of a mode rather than its wavelength and, from the resulting expression, calculate the difference in frequency between two successive longitudinal modes. La separazione in frequenza tra due modi longitinali adiacenti si ottiene dalla (5.1) e vale

$$\Delta\nu = c/2nL \qquad (5.2)$$

Free spectral range piano parallela

Per cavità piano parallela:
$\Delta\nu$ [GHz] ~ 1.5/(nL [m]) , con n indice rifrazione

$$\nu_r = \frac{c}{2d}\left[q + \frac{1}{2}(m + n + 1)\right] . \qquad (5.49)$$

The fundamental axial modes TEM_{00q} (m = n = 0) have the frequencies $\nu = (q+\frac{1}{2})c/2d$ and the frequency separation of adjacent axial modes is

$$\boxed{\delta\nu = \frac{c}{2d} .} \qquad (5.50)$$

Equation (5.49) reveals that the frequency spectrum of the confocal resonator is degenerated because the transverse modes with $q = q_1$ and $m+n = 2p$ have the same frequency as the axial mode with $m = n = 0$ and $q = q_1+p$. Between two axial modes there is always another transverse mode with (m+n+1) = odd. The free spectral range of a *confocal resonator* is therefore

$$\delta\nu_{confocal} = c/4d . \qquad (5.51)$$

Free spectral range confocale

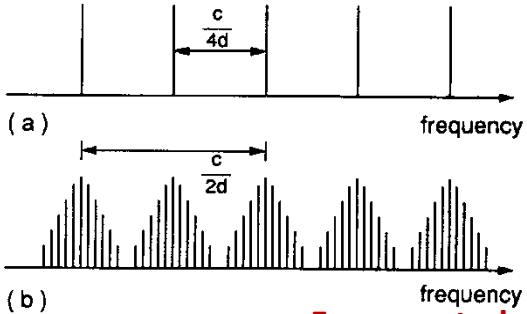

Free spectral range Confocale disallineata

Modi longitudinali cavità selezionano frequenze

Più modi longitudinali possono essere contemporaneamente sostenuti (separati da free spectral range)

SPETTRO DI GUADAGNO

Guadagno del mezzo attivo (sistema a tre livelli, da master equation):

$$\mathcal{G} = \frac{R(2A_{32}+A_{21}) - A_{21}(A_{31}+A_{32})}{A_{21}[A_{31}+A_{32}]}\left(\frac{c}{n}\right)\frac{N\hbar\omega B_{21} F(\omega)}{V}$$

Forma di riga del mezzo attivo

Il mezzo attivo permette guadagno all'interno di una certa banda

La condizione di conservazione dell'energia ($h\nu = E_2 - E_1$) deve essere rilassata
(lo è comunque nel caso in cui il mezzo attivo presenti *bande* di energia, come in alcuni solidi)

Principali cause di allargamento di riga:
- Allargamento **omogeneo** (tutti gli elementi si comportano statisticamente allo stesso modo)
- Allargamento **disomogeneo** (ogni elemento si comporta a modo suo e il risultato è "mediato")

Tipicamente:
- Allargamento omogeneo → forma di riga Lorentziana
- Allargamento disomogeneo → forma di riga Gaussiana
(in genere combinazione delle due)

LARGHEZZE DI GUADAGNO TIPICHE

Typical gain bandwidths:

Gain medium	Wavelength	Bandwidth (Hz)
HeNe	6328 Å	$1.5\ 10^{9}$
Nd:glass	1.06 μm	$3\ 10^{12}$
Nd:YAG	1.06 μm	$120\ 10^{9}$
Ruby	6943 Å	$6\ 10^{10}$
Argon ions	350 – 520 Å	$3.5\ 10^{9}$
Ti:Saphire	0.7-1.1 μm	$100\ 10^{12}$
Rh.-6G dye	0.56-0.64 μm	$5\ 10^{12}$
CO_2 gas	10 μm	$60\ 10^{6}$
Er doped fiber	1.55 μm	$4\ 10^{12}$
Diode lasers	0.7-1.6 μm	10^{13}

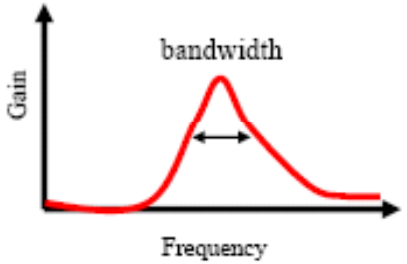

Esistono mezzi attivi con righe di guadagno “strette” (GHz) e larghe (THz)

Finestre di guadagno fino a centinaia di nm!

PRINCIPALI CAUSE ALLARGAMENTO OMOGENEO

Vita media (τ) finita dei livelli:
Ad esempio, se considero solo emissione spontanea, ho $\tau = \tau_{sp} = 1/A_{21}$

Principio di indeterminazione: $\Delta\omega\Delta t \geq 2\pi \rightarrow \Delta\omega \geq 2\pi/\tau$ (valori tipici per atomi in vapore/gas $\Delta\nu \sim$ 0.1 GHz)

Più realisticamente, a causa di processi di rilassamento (in genere non radiativi):
$1/\tau_{eff} = 1/\tau_{sp} + 1/\tau_{nonrad}$ → $\Delta\omega$ ~ 1-5 GHz, e anche oltre

Nota: processi non radiativi possono essere dovuti a collisioni interatomiche o intermolecolari nei vapori oppure a interazione con fononi nel caso di mezzi attivi a stato solido o liquido (larghezze omogenee grandi in questi casi!)

Si può dimostrare che la forma di riga in questi casi è Lorentziana con larghezza ~ $1/\tau_{eff}$
(cfr. anche forma di riga di ε_{R2} nell'interazione con dipolo classico smorzato, mod. Lorenz)

Esistono altri meccanismi di allargamento omogeneo, ad esempio per saturazione di potenza, quando $I >> I_{sat}$ (cfr. anche equazioni di bilancio per sistema a due livelli)

PRINCIPALI CAUSE ALLARGAMENTO DISOMOGENEO

3.2 Doppler Width

Generally the Lorentzian-line profile with the natural linewidth $\delta\nu_n$, as discussed in the previous section, cannot be observed without special techniques, because it is completely concealed by other broadening effects. One of the major contributions to the spectral linewidth in gases at low pressures is the Doppler width, which is due to the thermal motion of the absorbing or emitting molecules.

Consider an excited molecule with a velocity $\mathbf{v} = (v_x, v_y, v_z)$ relative to the rest frame of the observer. The central frequency of a molecular emission line that is ω_0 in the coordinate system of the molecule, is Doppler shifted to

$$\omega_e = \omega_0 + \mathbf{k}\cdot\mathbf{v} \tag{3.38}$$

for an observer looking towards the emitting molecule (that is, against the direction of the wave vector $\mathbf{k}$ of the emitted radiation; Fig.3.6a). The apparent emission frequency ω_e is increased if the molecule moves towards the observer ($\mathbf{k}\cdot\mathbf{v} > 0$), and decreased if the molecule moves away ($\mathbf{k}\cdot\mathbf{v} < 0$).

Similarly, one can see that the absorption frequency ω_0 of a molecule moving with the velocity $\mathbf{v}$ across a plane EM wave $\mathbf{E} = \mathbf{E}_0\exp(i\omega t - \mathbf{k}\cdot\mathbf{r})$ is shifted. The wave frequency ω in the rest frame appears in the frame of the moving molecule as

$$\omega' = \omega - \mathbf{k}\cdot\mathbf{v} .$$

The molecule can only absorb if ω' coincides with its eigenfrequency ω_0. The absorption frequency $\omega = \omega_a$ is then

$$\omega_a = \omega_0 + \mathbf{k}\cdot\mathbf{v} . \tag{3.39a}$$

As in the emission case the absorption frequency ω_a is increased for $\mathbf{k}\cdot\mathbf{v} > 0$ (Fig.3.6b). This happens, for example, if the molecule moves parallel to the wave propagation. It is decreased if $\mathbf{k}\cdot\mathbf{v} < 0$; e.g., when the molecule moves against the light propagation. If we choose the +z direction to coincide with the light propagation, (3.39a) becomes with $\mathbf{k} = (0,0,k_z)$ and $|k| = 2\pi/\lambda$,

$$\omega_a = \omega_0(1 + v_z/c) . \tag{3.39b}$$

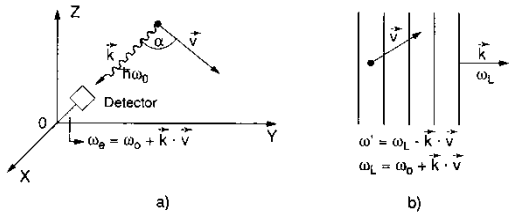

Fig.3.6. (a) Doppler shift of a monochromatic emission line and (b) absorption line

Note: Eqs.(3.38 and 39) describe the *linear* Doppler shift. For higher accuracies the quadratic Doppler effect has to be considered in addition (Sect.14.1).

At thermal equilibrium, the molecules of a gas follow a Maxwellian velocity distribution. At the temperature T, the number of molecules $n_i(v_z)dv_z$ in the level E_i per unit volume with a velocity component between v_z and v_z+dv_z is

$$n_i(v_z)dv_z = \frac{N_i}{v_p\sqrt{\pi}} e^{-(v_z/v_p)^2}\, dv_z , \tag{3.40}$$

where $N_i = \int n_i(v_z)dv_z$ is the density of all molecules in level E_i, $v_p = (2kT/m)^{1/2}$ is the most probable velocity, m is the mass of a molecule, and k is Boltzmann's constant. Inserting the relation (3.39b) between velocity component and frequency shift with $dv_z = (c/\omega_0)d\omega$ into (3.40) gives the number of molecules with absorption frequencies shifted from ω_0 into the interval from ω to $\omega+d\omega$

$$n_i(\omega)d\omega = N_i \frac{c}{\omega_0 v_p\sqrt{\pi}} \exp\left[-\left(\frac{c(\omega-\omega_0)}{\omega_0 v_p}\right)^2\right] d\omega. \tag{3.41}$$

Since the emitted or absorbed radiant power $P(\omega)d\omega$ is proportional to the density $n_i(\omega)d\omega$ of molecules emitting or absorbing in the intervall $d\omega$, the intensity profile of a Doppler-broadened spectral line becomes

$$I(\omega) = I_0 \exp\left[-\left(\frac{c(\omega-\omega_0)}{\omega_0 v_p}\right)^2\right] . \tag{3.42}$$

This is a Gaussian profile with a full halfwidth

$$\delta\omega_D = 2\sqrt{\ln 2}\,\omega_0 v_p/c = \left(\frac{\omega_0}{c}\right)\sqrt{8kT\ln 2/m} , \tag{3.43a}$$

which is called the *Doppler width*. Inserting (3.43) into (3.42) yields with $1/(4\ln 2) = 0.36$

$$\boxed{I(\omega) = I_0 \exp\left(-\frac{(\omega-\omega_0)^2}{0.36\,\delta\omega_D^2}\right).} \tag{3.44}$$

Note that $\delta\omega_D$ increases linearly with the frequency ω_0 and is proportional to $(T/m)^{1/2}$. The largest Doppler width is thus expected for hydrogen (M = 1) at high temperatures and a large frequency ω for the Lyman α line.

Equation (3.43) can be written more conveniently in terms of the Avogadro number N_A (the number of molecules per mole), the mass of a mole, $M = N_A m$, and the gas constant $R = N_A k$. Inserting these relations into (3.43) gives for the Doppler width

$$\delta\omega_D = (2\omega_0/c)\sqrt{2RT\ln 2/M} . \tag{3.43b}$$

or in frequency units, using the values for c and R,

$$\delta\nu_D = 7.16\cdot10^{-7}\,\nu_0\sqrt{T/M} \quad [\text{Hz}] . \tag{3.43c}$$

Example 3.2

a) Vacuum ultraviolet: For the Lyman α line ($2p \rightarrow 1s$ transition in the H atom) in a discharge with temperature T = 1000 K, M = 1, λ = 1216 Å, $\nu_0 = 2.47\cdot10^{15}\ s^{-1} \rightarrow \delta\nu_D = 5.6\cdot10^{10}$ Hz, $\delta\lambda_D = 2.8\cdot10^{-2}$ Å.

b) Visible spectral region: For the sodium D line ($3p \rightarrow 3s$ transition of the Na atom) in a sodium-vapor cell at T = 500 K, λ = 5891 Å, $\nu_0 = 5.1\cdot10^{14}\ s^{-1} \rightarrow \delta\nu_D = 1.7\cdot10^{9}$ Hz, $\delta\lambda_D = 1\cdot10^{-2}$ Å.

c) Infrared region: For a vibrational transition $(J_i,v_i) \leftrightarrow (J_k,v_k)$ between two rovibronic levels with the quantum numbers J, v of the CO_2 molecule in a CO_2 cell at room temperature (T = 300K), λ = 10 μm, $\nu = 3\cdot10^{13}\ s^{-1}$, $M = 44 \rightarrow \delta\nu_D = 5.6\cdot10^{7}$ Hz, $\delta\lambda_D$ = 0.19 Å.

Allargamento disomogeneo dominante in vapori/gas

Tipicamente $\Delta\nu$ ~ diversi GHz

Nel caso dei vapori/gas, il movimento (termico) degli atomi/molecole determina frequenze di risonanza effettive dipendenti dalla velocità (a causa di effetto Doppler)

Supponendo distribuzione velocità Maxwelliana (statistica di Boltzmann) si trova forma di riga Gaussiana

SPETTRO EMISSIONE LASER I

ser emission.

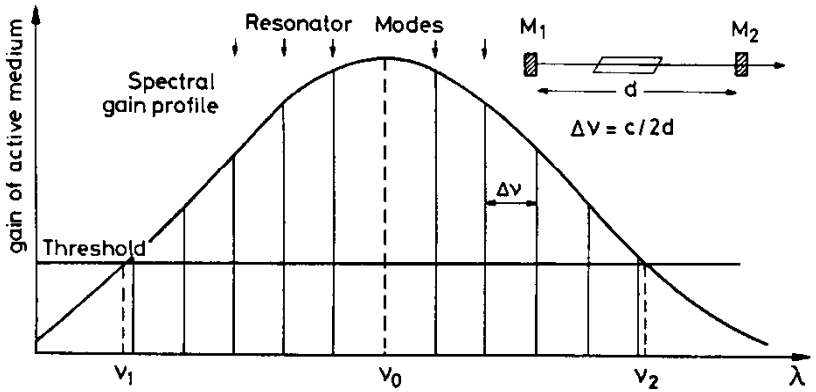

Fig.5.21. Gain profile of a laser transition with resonator eigenfrequencies c modes

According to (5.8) the gain profile $G_0(\nu) = \exp[-2\alpha(\nu)L]$ depends o the line profile $g(\nu-\nu_0)$ of the molecular transition $E_i \rightarrow E_k$. The threshol condition can be illustrated graphically by subtracting the frequency-de pendent losses from the gain profile. Laser oscillation is possible at all fre quencies ν_L where this subtraction gives a positive net gain (Fig.5.23).

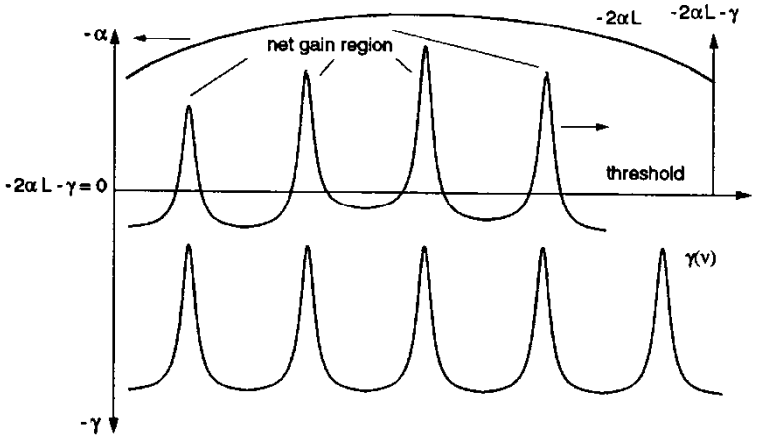

Fig.5.23. Reflection losses of a resonator (*lower curve*), gain curve $\alpha(\nu)$ (*upper curve* and net gain $\Delta\alpha(\nu) = -2L\alpha(\nu)-\gamma(\nu)$ as difference between gain ($\alpha < 0$) and losse (*middle curve*). Only frequencies with $\Delta\alpha(\nu) > 0$ reach oscillation threshold

5.3.1 Active Resonators and Laser Modes

Introducing the amplifying medium into the resonator changes the refrac- tive index between the mirrors and with it the eigenfrequencies of the reso- nator. We obtain the frequencies of the *active resonator* by replacing the mirror separation d in (5.52) by

$$d^* = (d-L) + n(\nu)L = d + (n-1)L\ , \tag{5.57}$$

where $n(\nu)$ is the refractive index in the active medium with length L. The refractive index $n(\nu)$ depends on the frequency ν of the oscillating modes, which are within the gain profile of a laser transition where anomalous dispersion is found. Let us at first consider how laser oscillation builds up in an active resonator.

If the pump power is increased continuously, threshold is reached first at those frequencies which have a maximum net gain. According to (5.5) the net gain factor per round trip

$$G(\nu, 2d) = \exp[-2\alpha(\nu)L - \gamma(\nu)]\ , \tag{5.58}$$

is determined by the amplification factor $\exp[-2\alpha(\nu)L]$ which has the fre- quency dependence of the gain profile (5.8), and also by the loss factor $\exp(-2\beta d/c) = \exp[-\gamma(\nu)]$ per round trip. While absorption or diffraction losses do not strongly depend on the frequency within the gain profiles of a laser transition, the transmission losses exhibit a strong frequency depend- ence, which is closely connected to the eigenfrequency spectrum of the resonator. This can be illustrated as follows:

Generalmente diversi modi longitudinali sono racchiusi nella forma di riga di guadagno

Risonatore attivo ha perdite grandi fuori dalle frequenze dei modi longitudinali (allargate in modo Lorentziano a causa della variazione di *n* con ω)

SPETTRO EMISSIONE LASER II

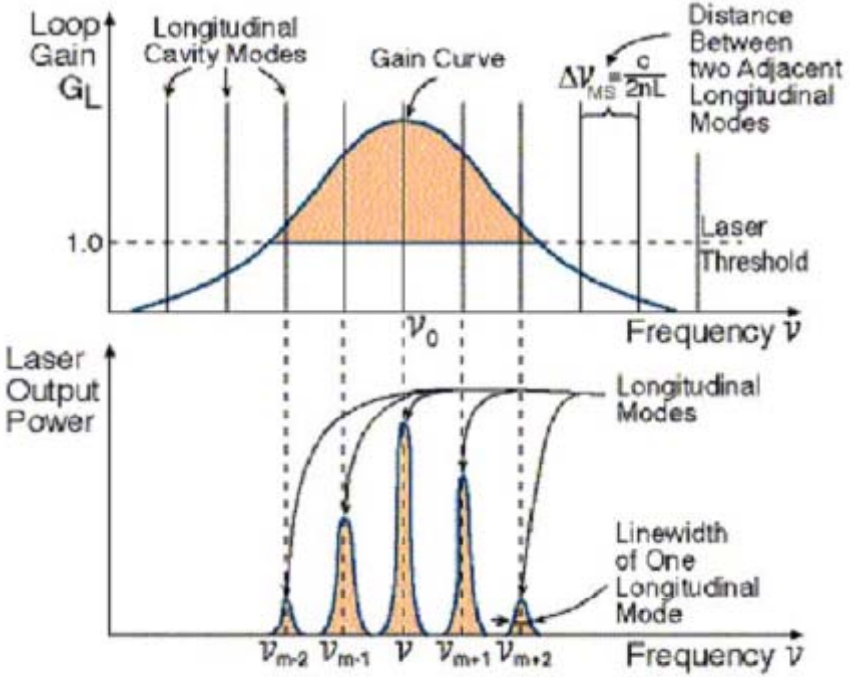

Lo spettro di emissione è determinato da convoluzione (o competizione?) di forma di riga di guadagno e modi cavità

Inoltre:

Il modo TEM_{00} presenta le minori perdite per diffrazione ed è, quindi, favorito nell'oscillazione laser. Gli altri modi di ordine superiore hanno ai bordi un'intensità più elevata del modo TEM_{00} e subiscono perdite per diffrazione maggiori. → Anche modo trasversale è selezionato

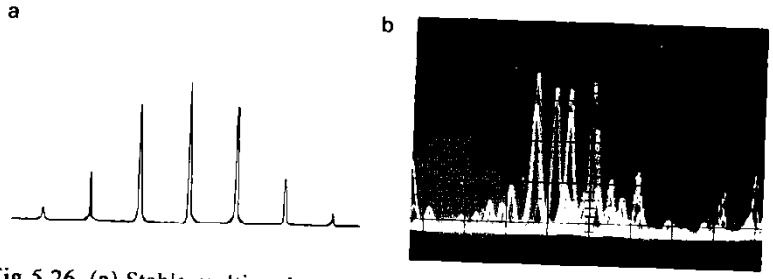

Fig.5.26. (**a**) Stable multimode operation of a HeNe laser. (Exposure time 1s): (**b**) Tv short-time exposures of the multimode spectrum of an argon laser superimposed the same film to demonstrate the randomly fluctuating mode distribution

Però operazione multimodo talvolta possibile come anche fluttuazioni random (jitter) in frequenza

ALCUNI ESEMPI DI CAVITÀ LASER

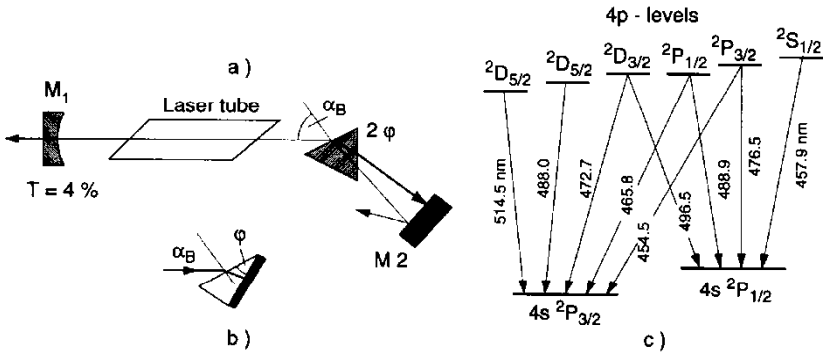

Fig.5.28. Line selection in an argon laser with a Brewster-prism (a) or a Littrow-prism reflector (b). Term diagram of laser transition in Ar^+ (c)

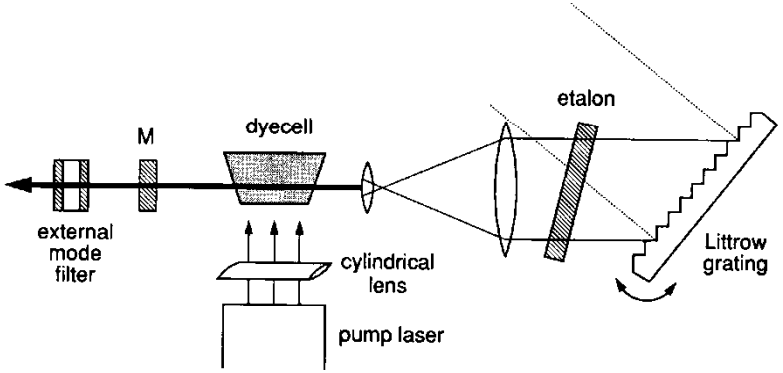

Fig.5.44. Short Hänsch-type dye-laser cavity with Littrow grating and mode selection either with an internal etalon or an external FPI as "mode filter" [5.57]

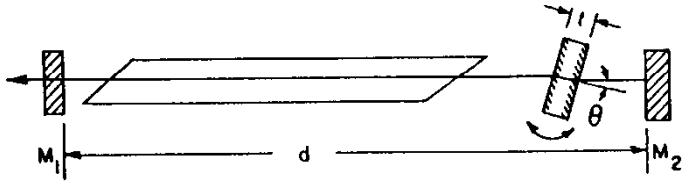

Fig.5.36. Single-mode operation by inserting a tilted etalon inside the laser resonator

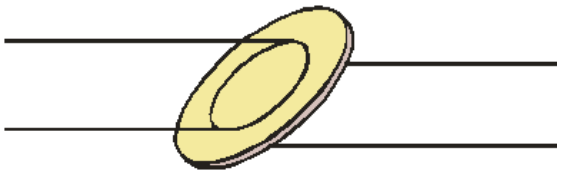

Figura 3.2: Bacchetta laser con le facce terminali tagliate all'angolo di Brewster.

CONCLUSIONI

Per creare una sorgente laser occorre inserire mezzo attivo (pompato) in una cavità ottica risonante, che è quindi componente essenziale del laser

Emissione laser ha luogo quando il guadagno del mezzo supera le perdite
→ esiste soglia per emissione laser

A causa delle condizioni al contorno, le cavità ottiche sostengono determinati modi di radiazione trasversali e longitudinali

Gli schemi più semplici (specchi piani paralleli) mostrano perdite per diffrazione

Schemi più complessi (e.g., confocali) aiutano a limitare le perdite

La selezione dei modi (longitudinali) influenza la lunghezza d'onda di emissione ed il carattere monocromatico

Vedremo in seguito quali caratteristiche della luce laser sono dovute direttamente alla cavità

FONTI

O. Svelto and P. Hanna, Principles of Lasers (Plenum Press, 1998)
http://www.wikipedia.org
R. Pratesi, *Dispense di Fisica dei Laser*, Università di Firenze ed INO, (http://www.ino.it/home/pratesi/DispenseL&A.htm).
http://people.seas.harvard.edu/~jones/ap216/lectures/ls_2/ls2_u5/ls2_unit_5.pdf
P.Burke, Lasers and Photonics, winter 2002 (uci.edu)